2008 American Control Conference
Westin Seattle Hotel, Seattle, Washington, USA
June 11-13, 2008

Model-Based Vibration Suppression in Piezoelectric Tube Scanners through Induced Voltage Feedback

Johannes Maess, Andrew J. Fleming, and Frank Allgöwer

Abstract— **The operation speed and tracking accuracy of piezoelectric tube actuators in scanning probe microscopy is significantly reduced due to the excitation of the scanner eigenfrequencies by the driving voltages. Feedback control is a suitable method for vibration suppression but suffers from the required additional sensor equipment and high cost for generation of a displacement feedback signal. Operating the piezotube in single-electrode excitation mode allows the comparatively uncomplex measurement of the induced voltages at sensor electrodes. The Finite Element (FE) approach enables an accurate modeling of the voltage signals. Furthermore, geometrical details included in the dynamic FE-model are the sample mass attached to the top of the tube as well as tube eccentricity and dislocated electrodes. Additionally, the FE-model accounts for dynamics-coupling effects along the separate axes of the three-dimensional tube motion. Comparison with experimental data demonstrates the accuracy of the FE-model. The controller employing the induced voltage as a feedback signal is designed by means of a reduced order model obtained from modal truncation. The efficacy of the controller is illustrated by closed-loop simulations.**

I. INTRODUCTION

Piezoelectric tube scanners are mainly used in micro- and nanopositioning tasks. A typical application is the relative positioning between the probe and sample in scanning probe microscopy and atomic force microscopy (AFM) [1]. This motion is divided in two parts, the lateral raster scan in the *xy*-plane and the topography tracking response in *z*-direction for AFM operation. From the piezoscanner setup depicted in Fig. 1, with four quartered outer electrodes and a grounded electrode deposited on the inner tube surface, the *xy*-scan motion is generated by applying the driving voltages v_{x} and v_{y} to the corresponding electrodes. The applied voltages give rise to a contraction of the tube area under the electrode surface by means of the indirect piezoelectric effect, inducing a bending motion of the tube, and finally resulting in a translation of the free end of the scanner along the respective axis [2], with the lower end being clamped. In the single-electrode excitation mode in Fig. 1 [3], the electrodes opposite to the potential electrodes are circuited in sensor configuration for measurement of the induced voltages $v_{\mathrm{ind,x}}$ and $v_{\mathrm{ind,y}}$ as output signals, generated by the direct piezoelectric effect.

Experiments were performed at the Laboratory for Dynamics and Control of Nanosystems, The University of Newcastle.

J. Maess and F. Allgöwer are with the Institute for Systems Theory and Automatic Control, Universität Stuttgart, Pfaffenwaldring 9, 70550 Stuttgart, Germany (email: {maess, allgower}@ist.uni-stuttgart.de).

A. J. Fleming is with the School of Electrical Engineering and Computer Science, The University of Newcastle, University Drive, Callaghan, NSW 2308, Australia (email: andrew.fleming@newcastle.edu.au).

The interest in such output signals is mainly motivated by the need of suitable feedback signals for closed-loop operation of piezoelectric tube scanners for enhancement of positioning precision [4] and increase in scan speed [5]. Contrary to displacement feedback signals employed e.g. in [6] and [7], requiring special displacement sensors, the induced voltages constitute output signals that are measurable without additional instrumentation and thus at comparatively low effort [8]. Other feedback approaches use the deflection signal of the AFM cantilever as feedback signal [9] and are thus restricted to the control of the *z*-displacement response. However, besides the nonlinear effects of hysteresis [10],[11] and creep [12], scan accuracy and scan speed are significantly limited by the excitation of the low-frequency structural resonances of the tube scanner [3] due to the driving voltages applied for *xy*-raster scan motion. The restrictions encountered in the aforementioned approaches demonstrate the need for easily measurable feedback signals for closed-loop control of the *xy*-motion.

Induced voltages in piezoelectric tube scanners have been investigated experimentally [2] and have been used as feedback signals for closed-loop vibration damping in [13]. In [13] as well as in other approaches [7], [5], the model of the piezoactuator describing the resonant behavior of a specific input-output configuration is identified from measurement data. In the article at hand, a linear dynamic model of the piezoelectric tube scanner is derived by Finite Element Analysis (FEA), representing a generalization to the identification procedure in terms of a complete description of the tube scanner dynamics. This modeling approach allows the simulation of induced voltage signals at sensor electrodes in the frequency and time domains. The induced voltage feedback controller can thus be designed from a model solely

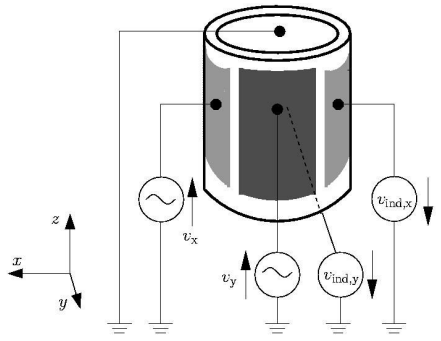

Fig. 1. Configuration of a piezoelectric tube scanner in single electrode excitation mode.

978-1-4244-2079-7/08/$25.00 ©2008 AACC.

based on geometrical data and material properties of the scanner. Additionally, the FEA enables a detailed modeling of the whole scan unit, consisting of the piezoelectric tube and a sample holder attached to its free end. Further effects included in the FE model describe tube imperfections resulting from machining tolerances in the manufacturing process, i.e. tube eccentricity [14] and dislocated electrodes not being centered above the respective *x*- or *y*-displacement axis. Both geometrical inaccuracies increase the dynamics-coupling between the scan axes in the three-dimensional scan motion. Compensation of dynamics-coupling-caused errors from the lateral *xy*-displacement to the perpendicular *z*-axis is treated in [15], whereas the FEA also accounts for coupling effects from *x*- to *y*-axis displacement. For controller design purposes, a model order reduction scheme [16] is applied to the FE model. The reduced order model accurately describes the scanner dynamics in the relevant frequency range.

II. Dynamic Modeling of Piezoelectric Tube Scanners

In the following, a detailed dynamical model of a piezoelectric tube scanner with a sample mass attached to the free end is derived from FE discretization and model order reduction. The model is vaildated by comparison to measured frequency response functions (FRF). Compared to models obtained from input-output derivation, the proposed FE model circumvents the tedious and error-prone process of model identification and additionally allows for predictions of the piezoscanner dynamics under design changes.

A. Finite Element Analysis

Modeling of piezoelectric tube scanners by FEA is so far restricted to a static analysis of the piezoelectric tube scanner [17] and of the tube assembly taking the sample holder into account [18]. The dynamic analysis of the piezoelectric tube in [19] is extended to the tube assembly in the present article. The fully-coupled structural and piezoelectric domains are described by the constitutive equations of the direct and indirect piezoelectric effects

$$\begin{aligned} \mathbf{T} &= \mathbf{c}^{\mathrm{E}}\mathbf{S} - \mathbf{e}\mathbf{E} \\ \mathbf{D} &= \mathbf{e}\mathbf{S} + \varepsilon^{\mathrm{S}}\mathbf{E}, \end{aligned}$$

where $\mathbf{T}$ denotes the mechanical stress matrix, $\mathbf{S}$ the mechanical strain matrix, $\mathbf{E}$ the electric field vector, $\mathbf{D}$ the electric charge vector per unit area, $\mathbf{c}^{\mathrm{e}}$ the mechanical stiffness matrix at constant electric field, ε^{S} the permittivity matrix under constant strain, and $\mathbf{e}$ the piezoelectric matrix. The equations of motion of order n in the FEA are given in the general formulation

$$\mathbf{M}\ddot{\mathbf{x}} + \mathbf{C}\dot{\mathbf{x}} + \mathbf{K}\mathbf{x} = \mathbf{F} \tag{1}$$

with mass matrix $\mathbf{M}$, damping matrix $\mathbf{C}$, stiffness matrix $\mathbf{K}$ and external loads $\mathbf{F}$. The physical states $\mathbf{x}$ consist of nodal displacements $\mathbf{u}$ and nodal electric potentials ϕ. To incorporate the structural boundary conditions at the clamped end of the piezotube and the electrical boundary conditions at the grounded, sensor and potential driving electrodes, the system of Eq. (1) is partitioned according to [20], leading to the mass and stiffness matrices $\mathbf{M}_{\mathrm{EV}}$ and $\mathbf{K}_{\mathrm{EV}}$. For a description of the input-output behavior of the model, all electrical degrees of freedom (DOFs) on each potential and sensor electrode are transformed into a single master degree of freedom, respectively. Further outputs considered are the nodal displacements at the top of the assembly in *x*-,*y*, and *z*-direction.

The $m \ll n$ low-frequency mode shapes ψ_r and the eigenfrequencies ω_r of Eq. 1 are obtained from solving the eigenvalue problem [16]

$$\mathbf{K}_{\mathrm{EV}}\psi_r = \omega_r^2\mathbf{M}_{\mathrm{EV}}\psi_r. \tag{2}$$

Tab. I quantifies the influence of the sample mass on the change of the eigenfrequencies of the tube assembly in comparison to the piezoelectric tube without sample mass [19]. The eigenfrequencies and the mode shape classification for the case without sample mass are given by the expressions in brackets in Tab. I. It is obvious that the resonances of the longitudinal bending modes are significantly shifted to lower frequencies due to the added mass effects of the sample mass. On the other hand, the sample holder glued on the free end of the tube causes local stiffening effects in the radial direction, resulting in higher eigenfrequencies of circumferential bending modes. Roughly speaking, the sample mass changes the mechanical boundary conditions of the piezoelectric tube from a clamped-free configuration to a clamped-clamped configuration with regard to the circumferential bending modes.

B. Model order reduction

Modal truncation [16] is applied for the derivation of the low order model. To this end, m low-frequency eigenmodes ψ_r are collected in the modal matrix Ψ. The system is transformed into modal coordinates $\mathbf{q}$ by the transformation law $\mathbf{x} = \Psi\mathbf{q}$. After normalization, the reduced mass matrix is given by the identity matrix with $\mathbf{I} = \Psi^{\mathrm{T}}\mathbf{M}_{\mathrm{EV}}\Psi \in \mathbb{R}^{m\times m}$, and the reduced stiffness matrix results in the spectral matrix $\Lambda \in \mathbb{R}^{m\times m}$ with $\Lambda = \Psi^{\mathrm{T}}\mathbf{K}_{\mathrm{EV}}\Psi = \mathrm{diag}\left(\omega_r^2\right)$ [16]. The resulting

TABLE I

Comparison of eigenfrequencies obtained from FEA for the tube assembly and piezoelectric tube without sample mass (bracketed expressions).

No.	Freq. [kHz]	Mode Shape Classification
1,2	0.83 (1.21)	1st Longitudinal Bending (1st Longitudinal Bending)
3,4	4.89 (6.49)	2nd Longitudinal Bending (2nd Longitudinal Bending)
5	5.72 (6.97)	Torsion (Torsion)
6	9.27 (11.30)	Longitudinal Extension (Longitudinal Extension)
7,8	12.28 (13.98)	3rd Longitudinal Bending (1st Circumferential Bending)
9,10	14.73 (14.50)	1st Circumferential Bending (2nd Circumferential Bending)
11,12	16.30 (15.38)	2nd Circumferential Bending (3rd Longitudinal Bending)

system is given as a set of second order decoupled differential equations. Finally, the system is expressed in modal state-space representation by

$$\begin{aligned} \dot{\mathbf{x}} &= \begin{bmatrix} \mathbf{0} & \mathbf{I} \\ -\Lambda & -\Gamma \end{bmatrix} \mathbf{x} + \begin{bmatrix} \mathbf{0} \\ -\Psi_{\mathrm{HSV}}^{\mathrm{T}} \mathbf{K}_{\mathrm{exc}} \end{bmatrix} \mathbf{u} \\ \mathbf{y} &= \begin{bmatrix} \mathbf{c}\Psi_{\mathrm{HSV}} & \mathbf{0} \end{bmatrix} \mathbf{x} \end{aligned} \tag{3}$$

where Γ denotes the damping term. In a multi-input, multi-output configuration, the inputs $\mathbf{u}$ are the driving voltages v_{x} and v_{y} applied to the potential electrodes. The physical outputs $\mathbf{y}$ are composed of the induced voltages at the sensor electrodes $v_{\mathrm{ind,x}}$ and $v_{\mathrm{ind,y}}$ described by the corresponding master DOF, and the nodal displacements u_{x}, u_{y} and u_{z} of a node located at the top of the tube assembly. The torsional mode shape in Tab. I does not contribute to the considered input-output behavior and is thus deleted from the truncation basis Ψ. Mathematically, this procedure is justified by the Hankel singular values (HSV) of the mode shapes [16], where the HSV obtained for the torsinal mode is significantly lower than the HSVs of the bending and longitudinal extension modes.

III. Results and Discussion

The simulated FRFs of the full and the reduced order FE-model are compared to measurement results for the displacement and induced voltage outputs. The reduced model is of order 12. The piezoelectric tube is operated in single-electrode excitation mode, with driving voltage v_{x}, and the y-axis potential electrode being grounded, corresponding to $v_{\mathrm{y}} = 0$.

A. Experimental description

The piezoelectric tube scanner manufactured from high-density PZT-5H (Boston PiezoOptics) is glued into a recessed aluminum base, and a sample mass is bonded to its free end as illustrated in Fig. 2(a). During measurement, the scan assembly is mounted on an optical table for isolation from external vibrations. Frequency responses of the scanner are measured with a Polytec PI PSV300 laser doppler vibrometer at the tip of the sample mass. The experimental parameters are given by a 5.5 Volt, 25 kHz bandwith periodic chirp driving signal at the potential electrodes and a sampling rate of 52.1 kHz for the measured signals. The FRFs are calculated from a 6400 line FFT. The geometrical parameters of the piezoelectric tube actuator are given in Fig. 2(b). A hollow aluminum cube with 10 mm edge length and 1.5 mm wall thickness, which is concentrically mounted on the tube by a fixation ring, is used as sample mass. The overall weight of the sample holder and the adhesive paste is 2.01 g.

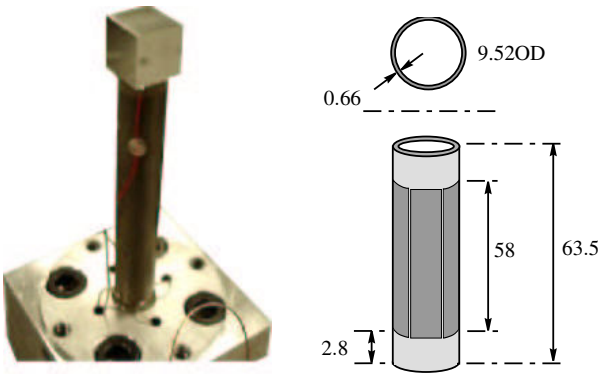

(a) Piezotube assembly. (b) Tube dimensions in mm.

Fig. 2. Measurement setup.

B. Displacement response

The displacement responses from the top of the sample holder are plotted in Fig. 3. A good agreement between the full FE-model and the measurement results is observed in the displacement outputs of all directions. Especially, high accuracy of the model is achieved for the x-displacement response in Fig. 3(a). In general, the model precisely matches the measurement around the longitudinal bending modes at 0.8 kHz, 4.9 kHz and 12.3 kHz, but shows some deviations around the circumferential bending modes. The reduced order model is valid in the frequency range up to approximately 15 kHz, in which most of 12 mode shapes of the truncation basis for the model reduction are located.

The displacement outputs in x- and y-direction in Fig. 3(a) and Fig. 3(b) are dominated by the first longitudinal bending mode at 0.83 kHz. The high amplification of its resonance typically limits the scan speed to 1/100 th of its eigenfrequency [8]. Compared to the x-axis displacement, only weak dynamics-coupling effects into the y-axis output occur, as observed from the fact of the amplitude response in Fig. 3(b) being approximately 40 dB lower than in Fig. 3(a).

The coupling effects from the x-excitation to the z-displacement output in Fig. 3(c) are significantly higher. Furthermore, the z-axis displacement is dominated by the resonance of the longitudinal extension mode at 9.3 kHz. The eigenfrequency of the longitudinal extension mode is also accurately matched by the FE models.

C. Induced voltage response

The simulated and measured FRFs for the induced voltage outputs are plotted in Fig. 4. Again, the comparison between simulated responses of the FE models and the experimental data shows a good agreement. In contrast to the displacement outputs of Fig. 3, the coupling effects between the x- and y-direction are strong for the induced voltages. This is obvious from the almost identical amplitudes in the FRFs of Fig. 4(a) and Fig. 4(b). It is interesting to note, that the induced voltages at the x- and y-electrodes significantly differ with respect to the amplification of the single mode shapes. In Fig. 4(a), the amplitude of the induced voltage at the x-sensor electrode shows articulate peaking in the frequency range of the first and second longitudinal bending modes. These longitudinal bending modes have only slight influence on the amplitude of the measured FRF at the y-sensor electrode in Fig. 4(b), while still being significant in the simulated response. In fact, the coupling term from the x-driving

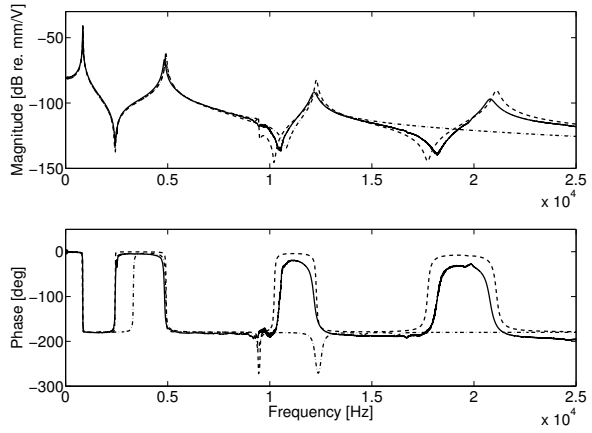

(a) x-displacement u_{x}.

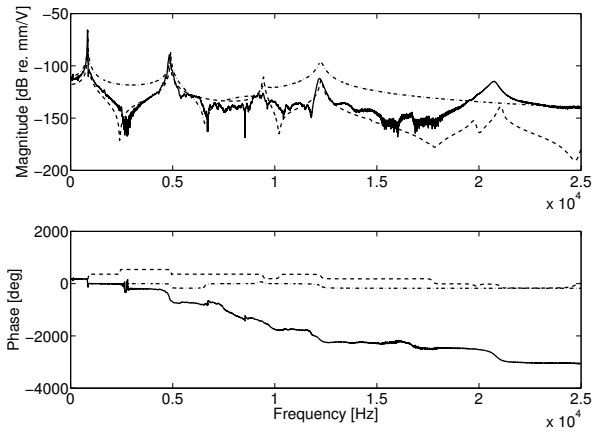

(b) y-displacement u_{y}.

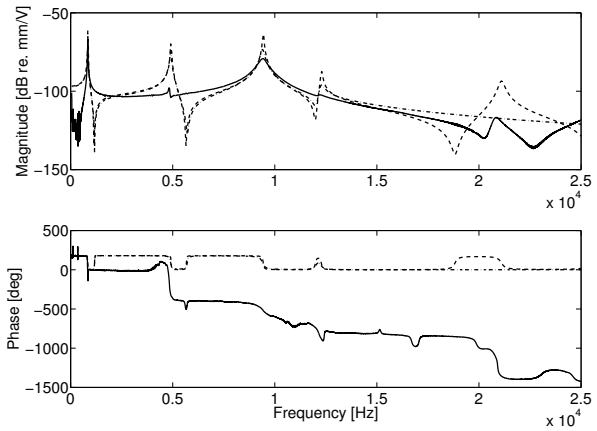

(c) z-displacement u_{z}.

Fig. 3. Comparison of FRFs for displacement outputs of measurement (solid curves), full finite element model (dashed curves), and reduced low order model (dashed-dottes curves).

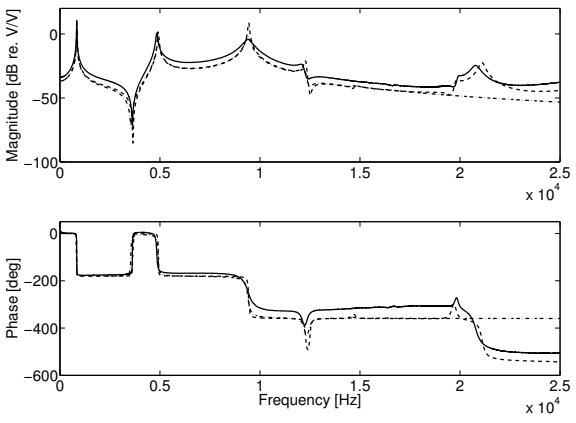

(a) Induced voltage $v_{\mathrm{ind,x}}$ at x-electrode.

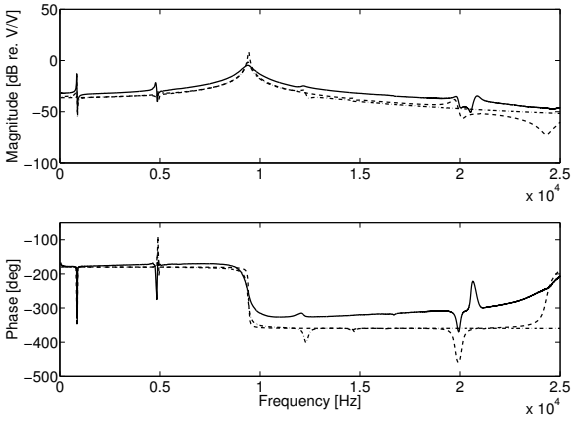

(b) Induced voltage $v_{\mathrm{ind,y}}$ at y-electrode.

Fig. 4. Comparison of FRFs for induced voltage outputs of measurement (solid curves), full finite element model (dashed curves), and reduced low order model (dashed-dottes curves).

voltage at the potential electrode to the induced voltage at the y-sensor electrode is dominated by the longitudinal extension mode at 9.3 kHz. This longitudinal extension mode also plays a significant role in the induced voltage at the x-sensor electrode. Since longitudinal extension is excited by any electrode input voltage, the corresponding mode has to be considered in closed-loop operation with induced voltage feedback signals. Furthermore, due to the strong coupling effects from x-axis voltage excitation to y-axis induced voltage, the design of SISO controllers for two-dimensional raster scan motion in the xy-plane is complicated. Another limitation in the design of model-based feedback controllers using the induced voltages as feedback signals lies in the non-collocated actuator-sensor configuration in the single electrode excitation case.

In summary, the FE model accurately describes the scanner dynamics with a sample mass attached to the top of

the tube and enables the simulation of dynamics-coupling effects. The second advantage over simple models derived from first-principle equations lies in the possibilty to simulate induced voltages at sensor electrodes with a precise description of the electrode shapes. The sensed voltages are used for model-based controller design in section IV.

IV. Induced Voltage Feedback Control

To simplify the control of the piezoelectric tube scanner by induced voltage feedback signals, only one-dimensional scanning motions are treated in the following. The *y*-axis reference trajectory is given by a triangular motion typically referred to as the fast scanning direction [8]. The corresponding *y*-axis raster scan motion composed of a staircase reference trajectory is discussed separately. Note that the staircase displacement is commonly replaced by a slowly increasing ramp signal of constant slope [21], imposing a considerable simplification of the raster scan trajectory tracking.

A. Controller design

A simple controller composed of a notch filter [7] and a PI-element is designed for trajectory tracking and prevention of induced vibrations. The notch filter of the form

$$G_{\mathrm{N}} = \frac{s^2 + 2\frac{d_1}{c_1}\omega_1 s + \omega_1^2}{s^2 + 2\frac{1}{c_1}\omega_1 s + \omega_1^2} \tag{4}$$

is used to compensate the first resonance frequency of the piezoelectric tube scanner at the angular frequency $\omega_1 = 2\pi \cdot 0.83 \cdot 10^3$ rad/s. The parameters c_1 and d_1 are adjusted to approximately match the amplitude of the resonance peak. The PI-controller $G_{\mathrm{PI}} = K_{\mathrm{p}}(1 + 1/(T_{\mathrm{I}}s))$ avoids steady-state errors in step signals. The corresponding parameters K_{p} and T_{I} are tuned to achieve a high bandwith of the closed-loop transfer function.

The overall controller takes the form $G_{\mathrm{c}} = G_{\mathrm{N}}G_{\mathrm{PI}}$. The bode plot of the controller is shown in Fig. 5 together with the bode plot of the plant corresponding to the transfer function from the *x*electrode driving voltage to the induced voltage $v_{\mathrm{ind,x}}$ in Fig. 4(a), and the resulting closed-loop transfer function. The notch filter damps the first resonance frequency for the input-output behavior under consideration. In fact, the notch filter removes the high-frequency components of the driving voltage signal and thus prevents the excitation of the tube resonance by the reference input. Robustness of the open-loop transfer function is characterized by a gain margin of 16.1 dB and a phase margin of 61.2°. It is pointed out that the presented low-complexity controller is highly robust to changes in high-frequency dynamics. Further improvement of tracking accuracy may be achieved by combining the simple controller with feedforward techniques.

B. Closed-loop simulations

In the experimental setup, an external resistance in the order of $r = 10 \cdot 10^6\ \Omega$ is included in the induced voltage measurement circuit. Together with the capacitance of the piezoelectric transducer $c = 10 \cdot 10^{-9}$ F, the resistance adds

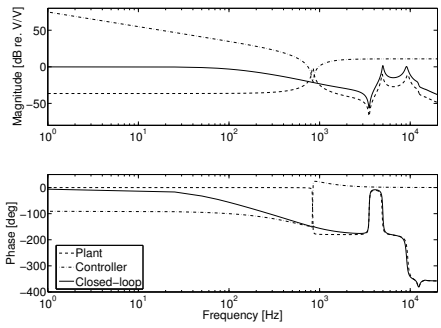

Fig. 5. Bode plots: plant, controller, and open-loop transfer function.

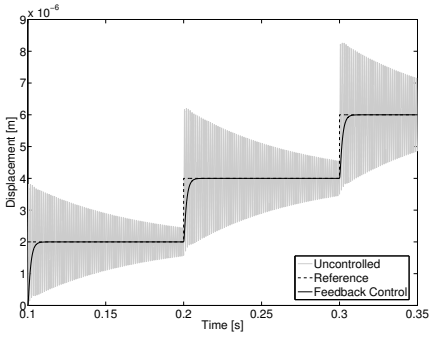

Fig. 6. Simulated displacements to staircase input voltage.

a high-pass filter with a cutoff frequency of approximately 1 Hz into the transfer function from the driving voltage to the induced voltage. This high-pass behavior is compensated for by a complementary low-pass filter, that is using the steady-state gain of the induced voltage signal as amplification of the input driving voltage [22]. The resulting control signal is then composed of the high-pass filtered transfer function signal for frequencies above 1 Hz and the steady-state response at low frequencies. This allows the designed controller to track offsets in the reference signal. To achieve a realistic simulation of induced voltage feedback operation, the described high- and low-pass filters are added to the model.

The simulated transient response to a staircase driving voltage is plotted in Fig. 6. In the uncontrolled case, the step responses are corrupted by strong structural vibrations of the piezoscanner. These vibrations are dominated by the weakly damped first longitudinal bending resonance, resulting in a slow amplitude reduction of the oscillation. In closed-loop operation, the steady-state value is reached after a time constant of approximately 0.01 s. The excitation of the first resonance mode by the driving voltage is suppressed by the notch filter. Thus, satisfactory tracking of the staircase motion of the raster scan is achieved by induced voltage feedback.

Fig. 7 shows the simulated displacement responses to a 10 Hz triangular voltage input. Again, induced vibrations are present in open-loop operation, but hardly visible in Fig. 7 due to the slow time scale. On the one hand, vibration

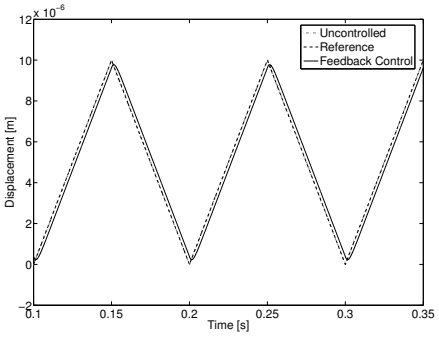

Fig. 7. Simulated displacements to triangular input voltage.

suppression is accomplished in closed-loop simulation. On the other hand, a significant time delay occurs in tracking of the triangular reference trajectory, which could be accounted for by feedforward compensation. An increase in feedback control bandwith for improvement of tracking accuracy is mainly limited by the growing controller complexity to suppress the excitation of the high-frequency resonances and by the non-collocated actuator/sensor configuration of the tube scanner.

V. Conclusions and Outlook

A comparison to measurement results demonstrates that accurate modeling of the dynamics of a piezoelectric tube scanner assembly consisting of the tube and a sample holder mounted to its free end over a wide frequency range is achieved by finite element analysis. This modeling approach allows the simulation of arbitrary displacement output signals as well as the determination of induced voltages at sensor electrodes. The applicability of the induced voltage as a feedback signal in closed-loop operation of piezoelectric tube scanners is revealed by simulation results for SISO trajectory tracking. The proposed controller achieves excellent vibration suppression for comparatively high-frequency driving voltages. The tracking accuracy of the controller is limited by its relatively low bandwith, due to the non-collocated configuration of the single-electrode excitation mode with induced voltage sensor electrodes.

In the experimental data as well as in the simulated frequency response functions, the induced voltage outputs show a strong coupling between motions in the lateral *xy*-plane. This coupling prevents the use of SISO controllers with induced voltage feedback for MIMO trajectory tracking. Further investigations thus include the design of MIMO controllers for two-dimensional raster scan motion and the application of inversion-based feedforward approaches [23] to induced voltage transfer functions. Furthermore, the extension of the FE-model of the piezoelectric scanner accounting for tube eccentricity, dislocated electrodes, and varying weight of the sensor holder is used to describe deviations from the nominal model. It is then possible to analyze controller robustness under induced voltage feedback by simulations with realistic model uncertainties.

References

[1] G. Binning and D. P. E. Smith, "Single-tube three-dimensional scanner for scanning tunneling microscopy", *Rev. Sci. Instr.*, vol. 57, no.8, pp. 1688-1689, 1986.

[2] W. F. Smith and B. W. Axelrod, "Measurements of the double piezoelectric effect", *Rev. Sci. Instr.*, vol. 71, no. 4, pp. 1772-1775, 2000.

[3] A. J. Fleming and S. O. R. Moheimani, "Sensorless vibration suppression and scan compensation for piezoelectric tube nanopositioners", *IEEE Trans. Contr. Syst. Techn.*, vol. 14, no. 1, pp. 33-44, 2006.

[4] D. Croft, G. Shed and S. Devasia, "Creep, hysteresis and vibration compensation for piezoactuators: Atomic force microscopy application", *Trans. ASME, J. Dyn. Syst. Meas. Contr.*, vol. 123, pp. 35-43, 2001.

[5] G. Schitter, F. Allgöwer, and A. Stemmer, "A new control strategy for high-speed atomic force microscopy", *Nanotechn.*, vol. 15, pp.108-114, 2004.

[6] N. Tamer and M. Dahleh, "Feedback control of piezoelectric tube scanners", in *Proc. 33rd Conf. Dec. Contr.*, Lake Buena Vista, CA, pp.1826-1831, 1994.

[7] K. K. Leang and S. Devasia, "Hysteresis, creep, and vibration compensation for piezoactuators: Feedback and feedforward control", in *2nd IFAC Conf. Mechatr. Syst.*, Berkeley, CA, pp. 283-289, 2002.

[8] S. S. Aphale, S. O. R. Moheimani, and A. J. Fleming, "Dominant resonant mode damping of a piezoelectric tube nanopositioner using optimal sensorless shunts", in *Proc. Amer. Contr. Conf.*, New York, NY, pp. 2220-2225, 2007.

[9] G. Schitter, A. Stemmer, and F. Allgöwer, "Robust 2DOF-control of a piezoelectric tube scanner for high speed atomic force microscopy", in *Proc. Amer. Contr. Conf.*, Denver, CO, pp. 3720-3725, 2003.

[10] M.-S. Tsai and J.-S. Chen, "Robust tracking control of a piezoactuator using a new approximate hysteresis model", *Trans. ASME, J. Dyn. Syst. Meas. Contr.*, vol. 125, pp.96-102, 2003.

[11] K. K. Leang and S. Devasia, "Design of hysteresis-compensating iterative learning control for piezo-positioners: Application to atomic force microscopes", *Mechatronics*, vol. 16, pp. 141-158, 2006.

[12] O. El Rifai and K. Youcef-Toumi, "Creep in piezoelectric scanners of atomic force microscopes", in *Proc. Amer. Contr. Conf.*, Anchorage, AL, pp. 3777-3782, 2002.

[13] M. Ratnam, B. Bhikkaji, A. J. Fleming, and S. O. R. Moheimani, "PPF Control of a piezoelectric tube scanner", in *Proc. 44th IEEE Conf. Dec. Contr., and Europ. Contr. Conf.*, Sevilla, Spain, pp. 1168-1173, 2005.

[14] O. M. El Rifai and K. Youcef-Toumi, "Coupling in piezoelectric tube scanners used in scanning probe microscopes", in *Proc. Amer. Contr. Conf.*, Arlington, VA, pp. 3251-3255, 2001.

[15] S. Tien, Q. Zou, and S. Devasia, "Iterative control of dynamics-coupling-caused errors in piezoscanners during high-speed AFM operation", *IEEE Trans. Contr. Syst. Techn.*, vol. 13, no. 6, pp. 921-931, 2005.

[16] W. K. Gawronski, *Advanced Structural Dynamics and Active Control of Structures*. New York: Springer-Verlag, 2004.

[17] R. G. Carr, "Finite element analysis of PZT tube scanner motion for scanning tunneling microscopy", *J. Micr.*, vol. 152, pp. 379-385, 1988.

[18] Q. Sun and R. A. Wolkow, "Three-dimensional displacement analysis of a piezoelectric tube scanner through finite element analysis of a tube assembly", *Rev. Sci. Instr.*, vol. 77, pp 113701 (1-9), 2006.

[19] J. Maess, A. J. Fleming, and F. Allgöwer, "Simulation of piezoelectric tube actuators by reduced finite element models for controller design", in *Proc. Amer. Contr. Conf.*, New York, NY, pages 4221-4226, 2007.

[20] J. Becker, O. Fein, M. Maess, and L. Gaul, "Finite element-based analysis of shunted piezoelectric structures for vibration damping", *Computers & Structures*, vol. 84, pages 2340-2350, 2006.

[21] D. Y. Abramovitch, S. B. Andersson, L. Y. Pao, and G. Schitter, "A tutorial on the mechanisms, dynamics, and control of atomic force microscopes", in *Proc. Amer. Contr. Conf.*, New York, NY, pp. 3488–3502, 2007.

[22] A. J. Fleming, A. Wills, and S. O. R. Moheimani, "Sensor fusion for improved control of piezoelectric tube scanners", in *IEEE/ASME Internatinal Conf. Advanced Intelligent Mechatronics*, Zurich, Switzerland, 2007.

[23] Q. Zou and S. Devasia, "Preview-based optimal inversion for output tracking: Application to scanning tunneling microscopy", *IEEE Trans. Contr. Syst. Techn*, vol. 12, pp. 375-386, 2004.